JACS
JOURNAL OF THE AMERICAN CHEMICAL SOCIETY

Article

pubs.acs.org/JACS

A Series of Layered Assemblies of Hydrogen-Bonded, Hexagonal Networks of C_3-Symmetric π-Conjugated Molecules: A Potential Motif of Porous Organic Materials

Ichiro Hisaki,[*,†] Shoichi Nakagawa,[†] Nobuaki Ikenaka,[†] Yutaka Imamura,[‡] Michio Katouda,[§] Motomichi Tashiro,[§] Hiromu Tsuchida,[∥] Tomoki Ogoshi,[∥] Hiroyasu Sato,[⊥] Norimitsu Tohnai,[†] and Mikiji Miyata[#]

[†]Department of Material and Life Science, Graduate School of Engineering, Osaka University, 2-1 Yamadaoka, Suita, Osaka 565-0871, Japan

[‡]Department of Chemistry, Graduate School of Science, Tokyo Metropolitan University, 1-1 Minami-Osawa, Hachioji, Tokyo 192-0397, Japan

[§]RIKEN Advanced Institute for Computational Science, 7-1-26 Minatojima-minami-machi, Chuo-ku, Kobe, Hyogo 650-0047, Japan

[∥]Graduate School of Natural Science and Technology, Kanazawa University, Kakuma-machi, Kanazawa 920-1192, Japan

[⊥]Rigaku Corporation, Matsubara-cho 3-9-12, Akishima, Tokyo 196-8666, Japan

[#]The Institute of Scientific and Industrial Research, Osaka University, 8-1 Mihogaoka, Ibaraki, Osaka 567-0047, Japan

Supporting Information

ABSTRACT: Hydrogen-bonded porous organic crystals are promising candidates for functional organic materials due to their easy construction and flexibility arising from reversible bond formation−dissociation. However, it still remains challenging to form porous materials with void spaces that are well-controlled in size, shape, and multiplicity because even well-designed porous frameworks often fail to generate pores within the crystal due to unexpected disruption of hydrogen bonding networks or interpenetration of the frameworks. Herein, we demonstrate that a series of C_3-symmetric π-conjugated planar molecules (**Tp**, **T12**, **T18**, and **Ex**) with three 4,4′-dicarboxy-*o*-terphenyl moieties in their periphery can form robust hydrogen-bonded hexagonal networks (H-HexNets) with dual or triple pores and that the H-HexNets stack without interpenetration to yield a layered assembly of H-HexNet (LA-H-HexNet) with accessible volumes up to 59%. Specifically, LA-H-HexNets of **Tp** and **T12** exhibit high crystallinity and permanent porosity after desolvation (activation): SA_{BET} = 788 and 557 $m^2\ g^{-1}$, respectively, based on CO_2 sorption at 195 K. We believe that the present design principle can be applied to construct a wide range of two-dimensional noncovalent organic frameworks (2D-nCOFs) and create a pathway to the development of a new class of highly porous functional materials.

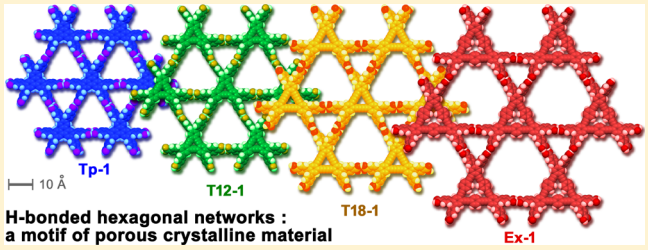

INTRODUCTION

Molecular-based porous materials are currently one of the central interests in the fields of material chemistry and crystal engineering.[1] A number of frameworks with various types of network topologies[2] and linkages (e.g., covalent,[3] dative,[4] and noncovalent[5] bonds) have been achieved. Among them, the two-dimensional hexagonal network (HexNet) is a facile and promising motif to access porous crystalline materials because a hexagonally networked 2D sheet can provide void spaces with well-predictable shapes in the sheet, and subsequent accumulation of the sheets without interpenetration forms a porous channel, as one can easily imagine. Indeed, HexNet structures composed of π-conjugated molecules have been applied to the storage of certain chemical species,[6] as platforms to build architectures inside voids,[7] and as photoelectronic materials.[8] In particular, layered assemblies of hydrogen-bonded HexNet (LA-H-HexNets) structures are attractive because they can be obtained by easy processes such as recrystallization, be precisely characterized by single X-ray analysis in many cases, and exhibit a reversible dynamic behavior originating from their structural flexibility.[9]

A pioneering example of a LA-H-HexNet is the layered honeycomb sheets of trimesic acid,[10] reported by Herbstein and co-workers in 1987 (Chart 1).[11] Using the appropriate solvent molecules prevented interpenetrated packing of the honeycomb network to yield layered assemblies. Since this work, LA-H-HexNets of trimesic acid have been applied as host frameworks to accommodate interesting guest species such as helicene.[6b] Tris(carboxylphenyl)benzene, an expanded analogue of trimesic acid, however, has not yielded a LA-H-HexNet, but instead forms nonporous crystals, in which solvent

Received: March 21, 2016
Published: May 1, 2016

ACS Publications © 2016 American Chemical Society

DOI: 10.1021/jacs.6b02968
J. Am. Chem. Soc. 2016, 138, 6617−6628

Chart 1. C_3- or C_6-Symmetric π-Conjugated Molecules with Hydrogen-Bonding Groups

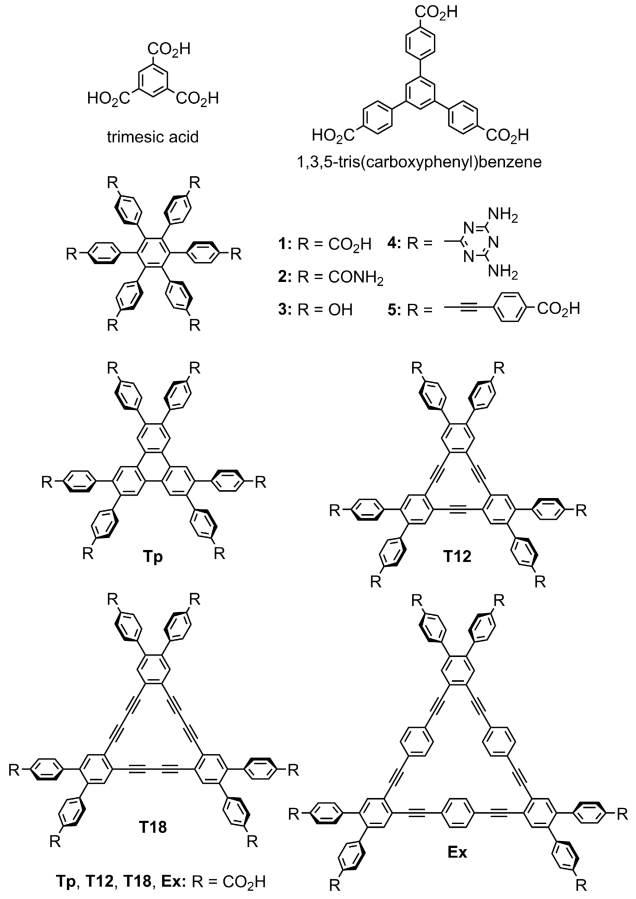

molecules such as dimethyl sulfoxide mask the carboxy groups through hydrogen bonding to prevent HexNet formation,[12] or HexNets assembled in an interpenetrated manner, excluding void spaces.[13] Remarkably, Kobayashi and co-workers demonstrated that hexakis(carboxyphenyl)benzene **1** formed a LA-H-HexNet, which was capable of including a naphthalene derivative in the void.[14] Subsequently, hexaphenylene substituted benzene derivatives **2**–**4** with hydrogen-bonding moieties were reported to form LA-H-HexNets,[15] indicating that hexaphenylene-substituted benzene derivatives are a crucial structure for yielding H-HexNets with uniformly shaped triangular voids. Disappointingly, however, the more expanded analogue **5** again yielded no porous H-HexNets and prevented formation of HexNets.[16] Therefore, it still remains challenging to establish a LA-H-HexNet with well-controlled void spaces in size, shape, and multiplicity, although many such porous layered HexNets have recently been achieved in 2D covalent organic frameworks (2D-COFs)[17] or as a monolayered H-HexNet on a surface.[18]

In connection with this, we designed C_3-symmetric π-conjugated building blocks (C_3PIs), namely, triphenylene, hexadehydrotribenzo[12]annulene, dodecadehydrotribenzo[18]annulene, and expanded cyclic phenylene ethynylene derivatives, **Tp**, **T12**, **T18**, and **Ex**, respectively (Chart 1), and planned to construct a series of LA-H-HexNets possessing multiple void spaces with systematically varied sizes and shapes. The working hypothesis to achieve LA-H-HexNets from C_3PIs is shown in Figure 1, which had been recently proposed by us.[19,20] First, for the central core of the building block, we

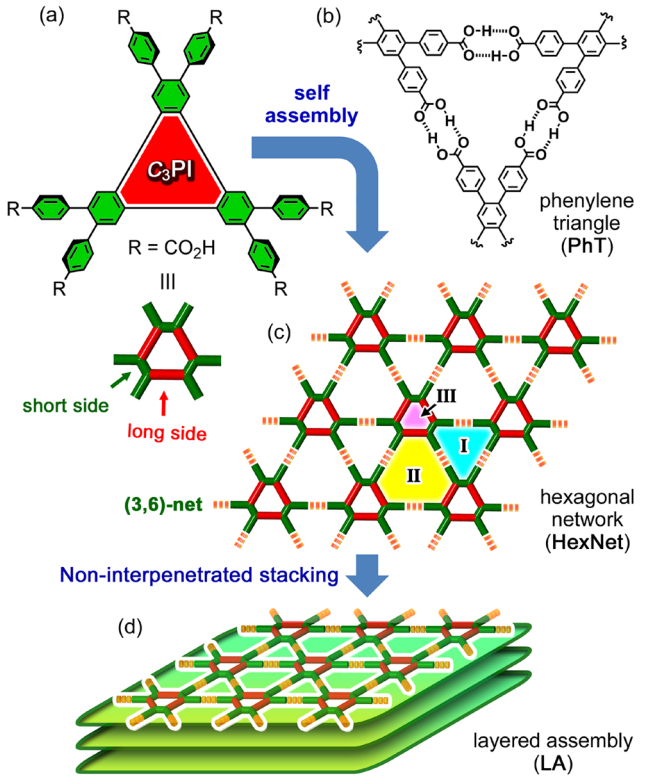

Figure 1. Construction of a layered assembly of hydrogen-bonded HexNet sheets (LA-H-HexNet). (a) C_3-symmetric π-conjugated molecules (C_3PIs) with 4,4′-dicarboxy-*o*-terphenyl moieties. (b) Phenylene triangle (PhT) motif. (c) Multiporous H-HexNet sheet. A C_3-symmetric macrocyclic molecule with alternate short and long sides provides three types of voids I, II, and III. (d) Layered assembly formed by stacking of the H-HexNet sheets without interpenetration.

applied a C_3-symmetric, rigid, planar core with sides of two different lengths, which enable the formation of a planar 2D HexNet motif with dual or triple void spaces. Moreover, the size and shape of the void can be varied by changing the side length of the C_3PI core. Second, in order to arrange C_3PIs into a hexagonally networked assembly with voids, three 4,4′-dicarboxy-*o*-terphenyl groups were placed on the periphery of the C_3PI core. The peripheral 4,4′-dicarboxy-*o*-terphenyl groups can form a hydrogen-bonded triangular porous motif, a so-called phenylene triangle (PhT) motif[19] to network the C_3PI. This group is also expected to increase solubility into a crystallization solvent and to prevent interpenetration of the H-HexNet sheet due to the nonplanar, sterically hindered phenylene moieties.

In this paper, we revealed for the first time that a series of C_3PIs formed isostructural H-HexNets with dual or triple void spaces with systematically varied sizes and shapes, and the H-HexNets were stacked in a different manner depending on the C_3PI to give the corresponding LA-H-HexNets. Furthermore, desolvated (activated) LA-H-HexNets of **Tp** and **T12** were revealed to retain the layered HexNet structure and permanent porosity.

We believe that the H-HexNets proposed here can be a solid motif for constructing noncovalently connected porous organic materials and that the results would create a pathway to the development of a new class of highly porous functional materials.

DOI: 10.1021/jacs.6b02968
J. Am. Chem. Soc. 2016, 138, 6617–6628

RESULTS AND DISCUSSION

Syntheses of C_3PI Molecules. **Tp** was prepared by the Suzuki-Miyaura coupling of 2,3,6,7,10,11-hexabromotriphenylene and 4-(methoxycarbonyl)-phenylboronic acid (**6**), followed by hydrolysis of the resulting hexamethyl ester **7** (Scheme 1a).[20] **T18** was synthesized according to Scheme 1b.

Scheme 1. Synthesis of (a) Tp and (b) T18

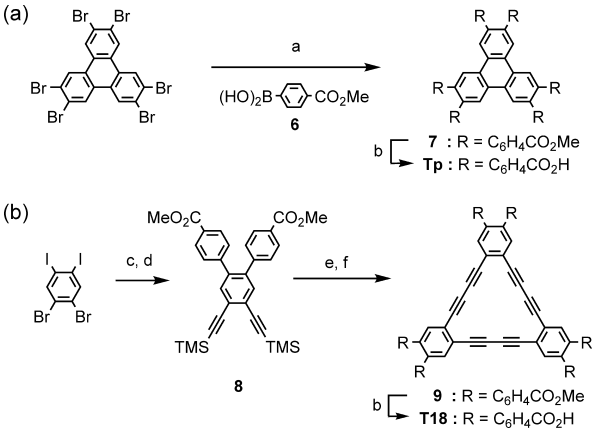

[a]Reagents and conditions: (a) **6**, $Ph(PPh_3)_4$, Na_2CO_3, toluene, MeOH, 1,4-dioxane, reflux, 46 h, 96%; (b) (1) KOH aq, THF, 50−60 °C, 37−50 h; (2) 6 M HCl, 93% for **Tp**, 90% for **T18**; (c) **6**, $Pd(PPh_3)_4$, K_3PO_4, 1,4-dioxane, reflux, 8 days, 31%; (d) TMSA, $Pd(PPh_3)_4$, CuI, Et_3N, 60 °C, 5 h, 89%; (e) TBAF, THF, rt, 1 h, 97%; (f) $Cu(OAc)_2$, pyridine, MeOH, ether, rt for 2 h, 60 °C for 0.5 h, rt overnight, 30%.

1,2-Dibromo-4,5-diidobenzene[21] was reacted with **6** under Suzuki-Miyaura coupling conditions, and subsequently reacted with trimethylsilylacetylene (TMSA) under Sonogashira coupling conditions to give diethynyl derivative **8**. Desilylation of **8** by tetrabutylammonium fluoride (TBAF), followed by oxidative coupling of the resulting terminal alkyne in the presence of Cu(II), yielded cyclic trimer **9**, which was then hydrolyzed to give **T18**.[19] **T12** and **Ex** were prepared according to Scheme 2. 3,4-Dibromoaniline was iodized by benzyltriethylammonium dichloroiodate (BTEA·ICl_2) in the presence of $CaCO_3$ to give a mixture of isomers **10a** and **10b** in a molar ratio of 76:24. The mixture of isomers was converted into the corresponding diethyl triazene derivatives (**11a** and **11b**), and column chromatography allowed isolation of pure **11a**. Sonogashira coupling of **11a** with triisopropylsilylacetylene (TIPSA), followed by Suzuki-Miyaura coupling of **12** with **6** gave **13**, which was treated with methyl iodide to give iodobenzene derivative **14**. Desilylation of **14**, followed by cyclotrimerization under Castro-Stephane reaction conditions, afforded triangular precursor **15**, which was subsequently hydrolyzed to yield **T12**. Iodobenzene derivative **14** was reacted with TMSA to yield **16**, which is desilylated and subsequently cross-coupled with **17** to yield **18**. Iodization of **18**, followed by desilylation of **19**, gave terminal acetylene monomer, which was cyclotrimerized to yield **20**. **Ex-1** was obtained by hydrolyzation of **20**. The absorption and fluorescence spectra of the C_3-PI molecules are shown in Figures S1 and S2, respectively, which is consistent with theoretical calculation (Figure S3.)

Crystallization of C_3PIs. To obtain LA-H-HexNet structures, building blocks (**Tp**, **T12**, **T18**, and **Ex**) were

Scheme 2. Synthesis of T12 and Ex

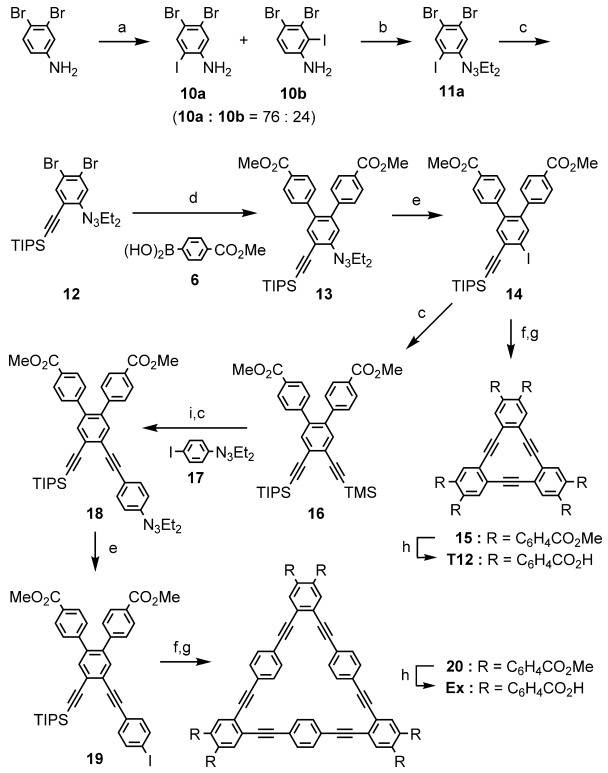

[a]Reagents and conditions: (a) BTEA·ICl_2, $CaCO_3$, $CHCl_3$, MeOH, reflux, 24 h; (b) (1) conc. HCl, CH_3CN, −5 °C; (2) $NaNO_2$, CH_3CN, water, −5 °C, 0.5 h; (3) Et_2NH, K_2CO_3, CH_3CN, water, −5 °C to rt, overnight, 78% from 3,4-dibromoaniline; (c) TIPSA for synthesis of **12**, TMSA for synthesis of **16**, **17** for synthesis of **18**, $Pd(PPh_3)_2Cl_2$, CuI, Et_3N or Et_3N/THF or iPr_2NH/THF, rt, 3−4 h, 96% for **12**, 96% for **16**, 78% for **18**; (d) **6**, $Pd(dppf)Cl_2$, Na_2CO_3, toluene, 1,4-dioxane, water, reflux, 24 h, 78%; (e) CH_3I, 130 °C, 36−40 h, 95% for **14**, 95% for **19**; (f) TBAF, THF, rt, 1.5 h; (g) (1) CuCl, NH_3 aq, EtOH, THF, rt, 3 h; (2) pyridine, reflux, overnight, 32% for **15** from **14**, 6% for **20** from **19**; (h) (1) KOH aq, THF, 50 °C, 15−20 h; (2) 6 M HCl, 97% for **T12**, 55% for **Ex**; (i) K_2CO_3, MeOH, ether, rt, 3 h, 90%.

crystallized under various conditions. The resultant optimized conditions are as follows (Scheme 3). **Tp** was crystallized by slow evaporation of a solution of *N*,*N*-dimethylformamide (DMF) and methyl benzoate (MeBz) at 100 °C to yield three polymorphic forms of LA-H-HexNet (**Tp-1**, **Tp-2**, and **Tp-3**).[20] Forms **Tp-1** and **Tp-2** were frequently formed

Scheme 3. Optimized Crystallization Conditions for Formation of the LA-H-HexNets

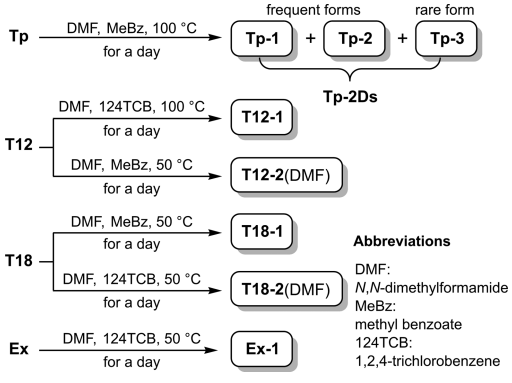

DOI: 10.1021/jacs.6b02968
J. Am. Chem. Soc. 2016, 138, 6617−6628

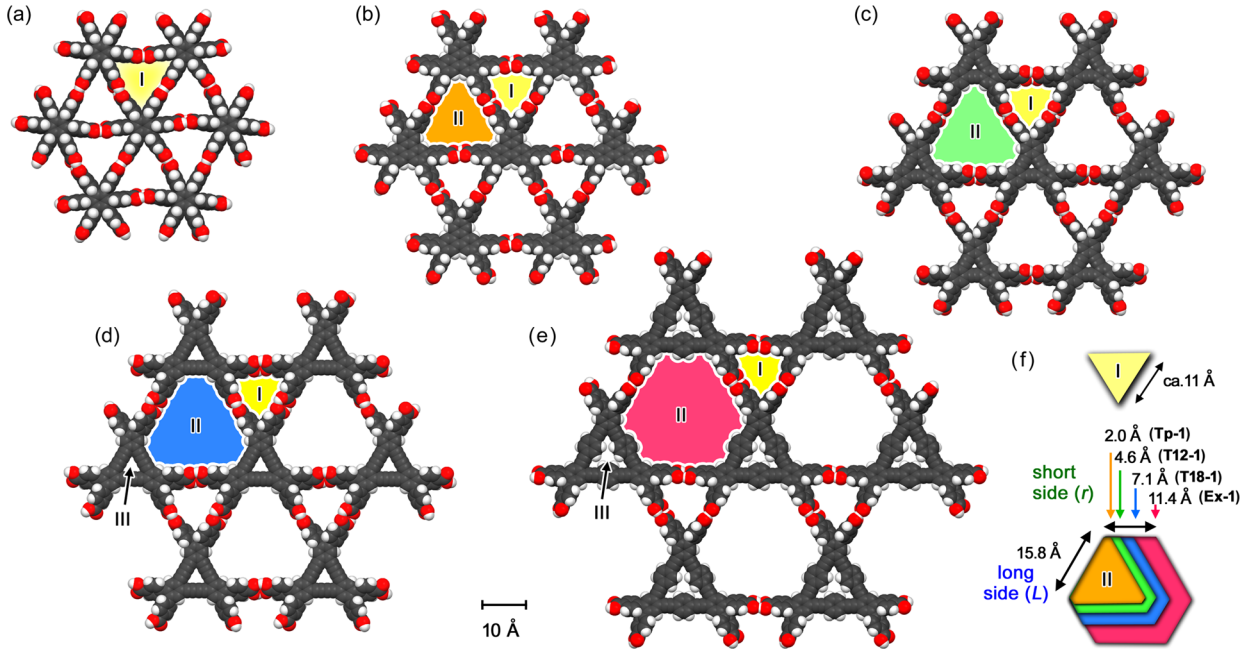

Figure 2. Crystal structures of H-HexNet motifs of (a) Kobayashi's molecule **1** (CSD RefCode: DOCLIQ), (b) **Tp-1**, (c) **T12-1**, (d) **T18-1**, and (e) **Ex-1**. (f) Dimensions of void I (top) and II (bottom). The latter depends on the size and shape of C_3PI molecular cores. Cyclic C_3PI core also provides intrinsic void space (III) within the molecule.

Table 1. Structural Parameters of the LA-H-HexNets

	1	Tp-1	T12-1	T18-1	Ex	T12-apo
Z' value	1	1	2	3	1	1
ω [deg][a]	85.2−88.6	54.7−76.0	42.4−88.9	34.8−59.6	44.7−63.6	19.1−84.4
	ave. 86.4	ave. 59.4	ave. 51.3	ave. 49.4	ave. 51.03	ave. 58.8
ψ [deg][b]	-	46.6	37.4[c]	69.1[c]	53.9	-
L (Å)/r (Å)[d]	-	15.8/2.0	15.8/4.6	15.8/7.1	15.8/11.4	15.8/4.6
accessible volume[e]	46%	54%	41%	58%	59%	38%
(h k l) plane for HexNet	(2 0 1)	(1 1 −1)	(1 1 1)	(1 0 0)	(2 1 −1)	(2 0 −1)

[a]Averaged dihedral angle of carboxyphenyl groups against the C_3PI core (see Figure 3a). [b]Twisted angle of carboxyphenyl dimer at the frustration (see Figure 3a). [c]Averaged values. [d]L: length of longer side. r: length of shorter side. The length of the sides refers to the distance between the aromatic hydrogen atoms at the *ortho*-position of the carboxyphenyl substituent. [e]Calculated by PLATON software.

concomitantly or individually depending on crystallization batches, while **Tp-3** was rarely obtained.[20] Since the H-HexNet sheets in the polymorphs have the same topology and are stacked in nearly the same way, only the structure of **Tp-1** is shown as a typical example. **T12** was crystallized by slow evaporation of a DMF and 1,2,4-trichlorobenzene (124TCB) solution at 100 °C to yield LA-H-HexNet crystal **T12-1**.[22] **T18** and **Ex** also yielded LA-H-HexNet crystals **T18-1**[19] and **Ex-1**[22] by slow evaporation of DMF/MeBz and DMF/124TCB solutions, respectively, at 50 °C. It is noteworthy that crystallization without poor solvents or at low temperature, such as room temperature, yielded no H-HexNet structure but partially networked structures, in which the carboxy groups were hydrogen bonded by DMF molecules, preventing hexagonal network formation (Figure S4).

H-HexNet Structures of C_3PIs. The obtained H-HexNet structures of the C_3PIs (**Tp**, **T12-1**, **T18-1**, and **Ex**) are shown in Figure 2, together with that of **1**[14] as a reference. All members yielded porous H-HexNet structures through formation of the hydrogen-bonded PhT motif as we expected. The PhT motif involves a triangular void space with a side length of ca. 11 Å (pore-I). C_6-symmetric **1** resulted in formation of pore-I uniquely. Other members with C_3-symmetry, on the other hand, afforded both pore-I and another larger pore (pore-II) with a nonregular hexagonal shape, whose dimensions varied depending on the size of the C_3PI cores (Figure 2f and Table 1). The longer sides of pore-II are the same (L = 15.8 Å) in the four systems, while the shorter sides (r) ranged from 2.0 to 11.4 Å. Therefore, pore-II of **Tp-1** has a nearly triangular shape, while that of **Ex-1** has a nearly hexagonal one. Additionally, cyclic C_3PI molecules (**T12**, **T18**, and **Ex**) can provide a third void (pore-III) because of the intrinsic pores within the molecules. Although pore-III of **T12** is too narrow to accommodate a molecule, that of **T18** has a diameter of 3.5 Å, and that of **Ex** has a diameter of 7.4 Å when the phenylene ring of **Ex** is perpendicular to the molecular plane. These results demonstrate that rigid C_3-symmetric cyclic molecules equipped with 4,4′-dicarboxy-*o*-terphenyl moieties can readily construct a wide range of H-HexNet structures possessing multiple pores with various shapes and sizes.

Despite the robustness of the HexNet topology, carboxyphenyl groups have rotational flexibility, allowing various rotational conformations in the crystals. The conformation is closely related to the stacking manner of the H-HexNet sheets as described later. The dihedral angles of the carboxyphenyl groups (ω) against the C_3PI core observed in the crystals are

DOI: 10.1021/jacs.6b02968
J. Am. Chem. Soc. 2016, 138, 6617−6628

listed in Table 1. The carboxy phenyl groups in **1** are nearly perpendicular to the central core (ω = 86.4°) because of steric hindrance. The other C_3PIs, on the other hand, have relatively small values of ω ranging from 49.4° to 59.4°. Because of the inclined conformation of the carboxyphenyl groups, the PhT motif is forced to include conformational frustration in at least one of the hydrogen-bonded moieties (Figure 3a). PhT motifs

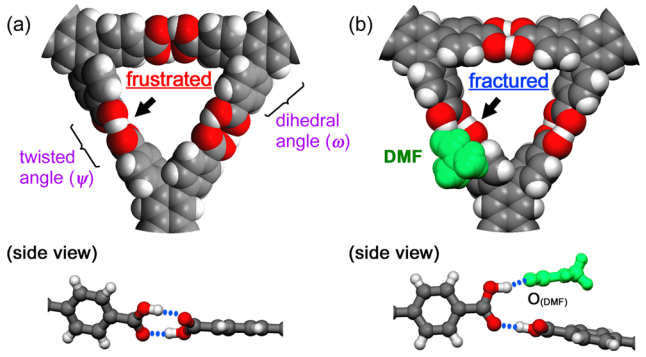

Figure 3. Hydrogen bonded phenylene triangle (PhT) motif. (a) PhT with conformationally frustrated hydrogen-bonded dimer. (b) PhT with hydrogen-bonded DMF molecule, which releases the frustration.

of **Tp-1**, **T12−1**, **T18−1**, and **Ex-1** have frustration in one of three hydrogen bonds. The dihedral angles between hydrogen-bonded carboxyphenyl groups (ψ) are 46.6°, 37.4°, 69.1°, and 53.9°, respectively. To release the frustration, a solvent molecule such as DMF is sometimes inserted into the frustrated part through hydrogen bond formation (Figure 3b). Such insertion was brought about by subtle changes in the crystallization conditions. For example, crystallization of **T18** with 124TCB instead of MeBz yielded DMF-inserted LA-HexNet crystal **T18-2**(DMF) (Figure S5a). Similarly, crystallization of **T12** with MeBz instead of 124TCB at 50 °C yielded **T12-2**(DMF) (Figure S5b). Since the DMF-inserted LA-HexNet crystals exhibit the same thermal behavior as that of the DMF-free LA-HexNets crystal, we will only discuss the latter LA-HexNets in the following setions.

Layered Structures of H-HexNet Sheets. Selected layered structures (three layers) of H-HexNet sheets in **Tp-1**, **T12-1**, **T18-1**, and **Ex-1** are shown in Figure 4a−d. In general, a low density framework tends to form an interpenetrated structure to fill empty spaces.[13] However, the present H-HexNet sheets are stacked without interpenetration to retain void spaces, in which aromatic molecules used in crystallization are accommodated. Some of the included molecules were capable of being refined crystallographically and the others were not because of severe disorder within the void, although they are omitted in Figure 4 for clarity. The accessible void spaces evaluated by the PLATON software are 54% for **Tp-1**, 41% for **T12-1**, 58% for **T18-1**, and 59% for **Ex-1**.[23]

Remarkably, H-HexNet layers in the crystal structures are not perfectly overlapped, which is different from the eclipse stacking reported in most 2D-COFs.[24] The eclipse stacking may be uncomfortable for H-HexNet layers due to steric hindrance of the phenylene moieties attached to the periphery of the C_3PI cores. The present crystals hence belong to space group $P\bar{1}$ and the H-HexNet layers are stacked in a XX′ manner, where X and X′ layers are related by inversion symmetry (Figure 4e). Furthermore, crystals **T12-1** and **T18-1** include two and three crystallographically independent C_3PI molecules (Z' = 2 and 3), respectively, and each of the independent molecules individually composes a H-HexNet sheet. Therefore, the X layers of **T12-1** and **T18-1** consist of two layers (A and B in Figure 4f) and three layers (A, B, and C in Figure 4g), respectively. To reveal the layered structures in more detail and compare them among the four systems, stacking manners of the rhombic motifs were carefully investigated.

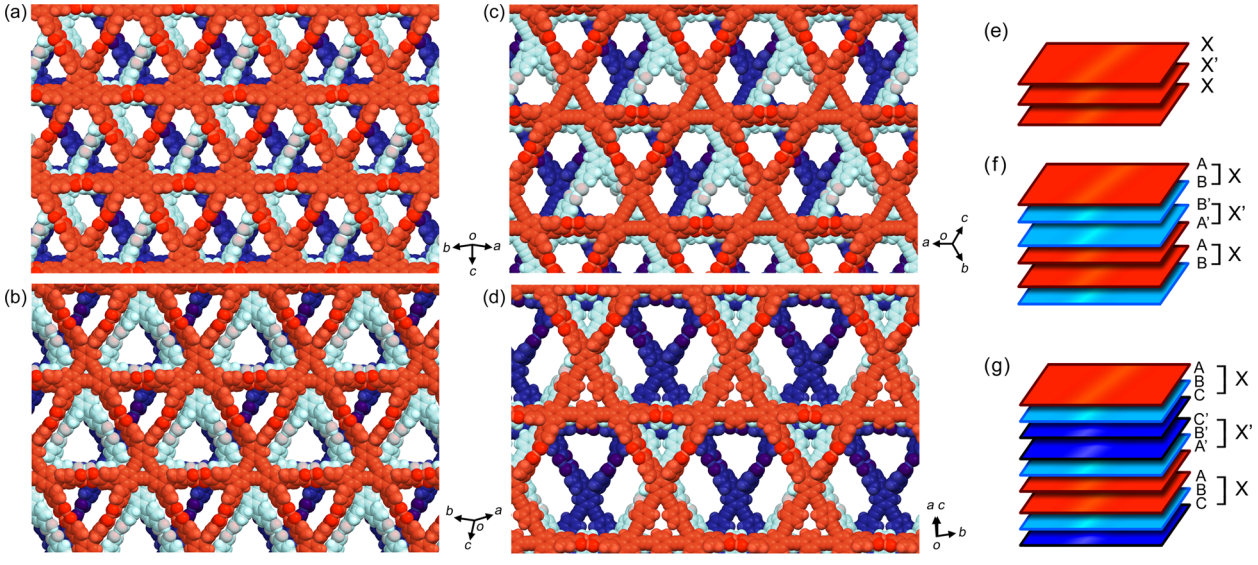

Figure 4. Crystal structures of LA-H-HexNets (a) **Tp-1**, (b) **T12-1**, (c) **T18-1**, and (d) **Ex-1**, viewed from above the H-HexNet sheet. The H-HexNet sheets of **Tp-1**, **T12-1**, **T18-1**, and **Ex-1** are laid parallel to the (1 1 −1), (1 1 1), (1 0 0), and (2 1 −1) planes, respectively. The first, second, and third layers are colored red, light cyan, and dark blue, respectively. The solvent molecules in the voids are omitted for clarity. Schematic representations of stacking manners of the H-HexNet layers: (e) **Tp-1** and **Ex-1** with Z' = 1, (f) **T12-1** with Z' = 2, and (g) **T18-1** with Z' = 3. In the case of a system with Z' = 1, a layer X contains one HexNet layer. In the case of a system with Z' = 2 or 3, a layer X consists of A- and B-layers or A-, B-, and C-layers, respectively, where each of A-, B-, C-layers are composed of individual crystallographically independent molecules. X and X′ are related by inversion symmetry. Z' indicates the number of crystallographically independent molecules included in the cell.

DOI: 10.1021/jacs.6b02968
J. Am. Chem. Soc. 2016, 138, 6617−6628

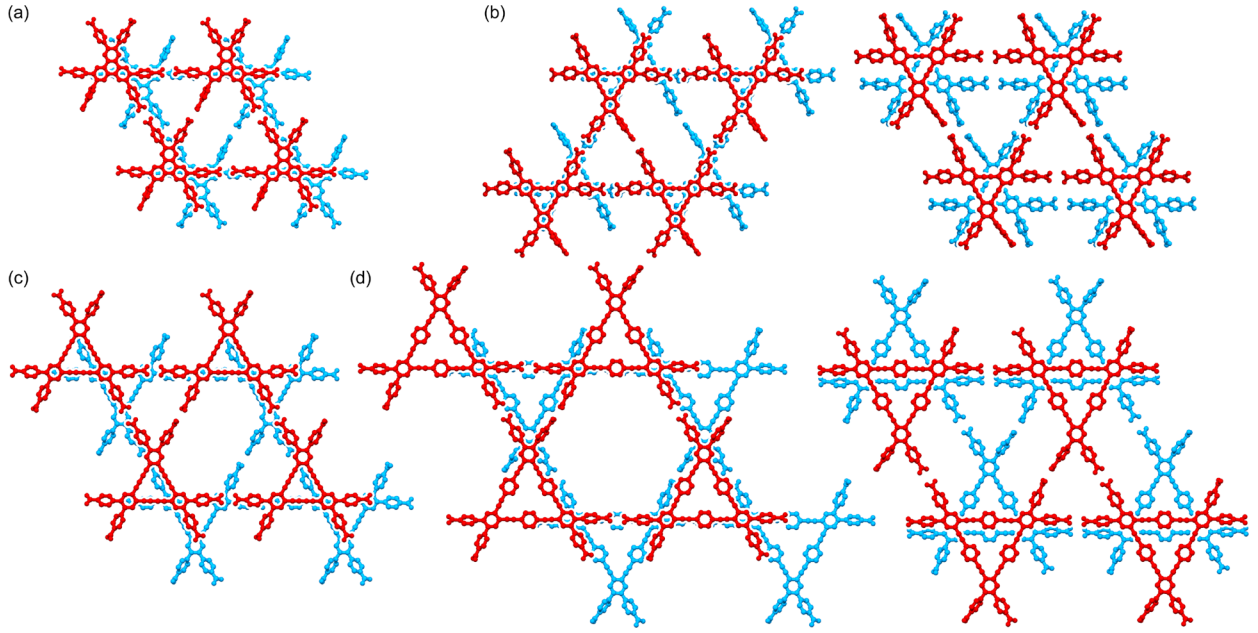

Figure 5. Typical stacking manners of the two adjacent rhombic motifs observed in (a) **Tp-1**, (b) **T12-1**, (c) **T18-1**, and (d) **Ex-1**. (a, b-left, and c) The outer parts of the rhombic frames are superimposed with each other (rhomb-frame stacking). (b-right and d-right) The C_3PI cores have large overlap with obvious $\pi-\pi$ stacking interactions (π-core stacking). (d-left) The layers are stacked with nearly perfect overlap of the frames (eclipse stacking).

Figure 5 shows typical examples of the bilayer stacking manners observed in **Tp-1**, **T12-1**, **T18-1**, and **Ex-1**. Although LA-H-HexNet crystals with $Z' = 1$, 2, and 3 strictly include two, four, and six patterns of the stacking manners as shown in Figures S6–S9, they can be classified by the patterns shown in Figure 5 (for details, see Supporting Information). **Tp-1** and **T18-1** have closely related stacking manners (Figure 5, panels a and c, respectively): the neighboring rhombic frames are nearly eclipsed or slightly slipped-stacked so as to superpose the outer parts of the rhombic frames with each other (so-called rhomb-frame stacking). **Tp-1** has an averaged interlayer distance of 4.7 Å. The interlayer interactions are self-complementary CH···O contacts between hydrogen atoms of the phenylene groups and oxygen atoms in the carboxy groups and CH···π contacts between the phenylene groups and triphenylene plane (Figure S10).[20] **T18-1** has an averaged interlayer distance of 4.1 Å. The intermolecular interactions are CH···π contacts between the carboxyphenyl group and the **T18** core and small $\pi\cdots\pi$ contacts between slightly overlapped **T18** cores (Figure S12). Rotational flexibility of the carboxyphenyl groups contribute to optimization of stacking conformations to form effective interlayer interactions such as CH···π interactions. **T12-1**, on the other hand, has a large overlap of the **T12** cores with obvious $\pi\cdots\pi$ stacking interactions with a distance of 3.0 Å (so-called π-core stacking), as shown in Figures 5b (right), in addition to the rhomb-frame stacking [Figure 5b (left)]. The π-core stacking manner in **T12-1** results in generation of two trigonal void spaces within the rhombic bilayer. Stacking manners of HexNets in **Ex-1** are completely different from the others as shown in Figure 5d (left). Although the two adjacent layers are related by an inversion center as observed in the other systems, the XX′ layers are stacked with perfect overlap of the frames (so-called eclipse stacking) due to accordance in the size and shape between the cyclic **Ex** core and the PhT motif, giving a large hexagonal void space. Again, the rotational flexibility of the carboxyphenyl groups and the phenylene groups in the core adopts a suitable conformation to form effective interlayer interactions. (Figure S13). **Ex-1** also includes stacking between the horizontal parts of the π-cores through $\pi\cdots\pi$ interactions as shown in Figure 5d (right). In this way, the systematic comparison revealed that the stacking manners of the H-HexNets are crucially affected by the size of the π-conjugated cyclic cores, although a series of C_3PIs form H-HexNet structures with the same topology.

Thermal Behaviors of the As-Formed Crystals. Freshly prepared crystalline bulks of **Tp-2Ds** (which contains both or either of **Tp-1**, **Tp-2**, or/and **Tp-3**),[20,25] **T12-1**, **T18-1**, and **Ex-1** were subjected to thermal analyses (Figure 6). ^{1}H NMR spectra (Figures S14, S16, S17, and S18) and Thermogravimetric (TG) analysis revealed the host–guest ratios in the LA-H-HexNet crystals: **Tp**/MeBz = 1/6 for **Tp-2Ds**; **T12**/

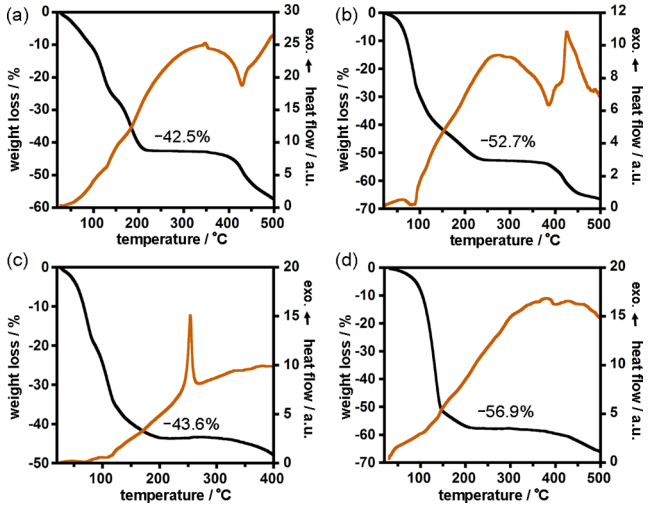

Figure 6. Thermal analyses of (a) **Tp-2Ds**, (b) **T12-1**, (c) **T18-1**, and (d) **Ex-1**. TG curve, black; DTA curve, orange.

DOI: 10.1021/jacs.6b02968
J. Am. Chem. Soc. 2016, 138, 6617–6628

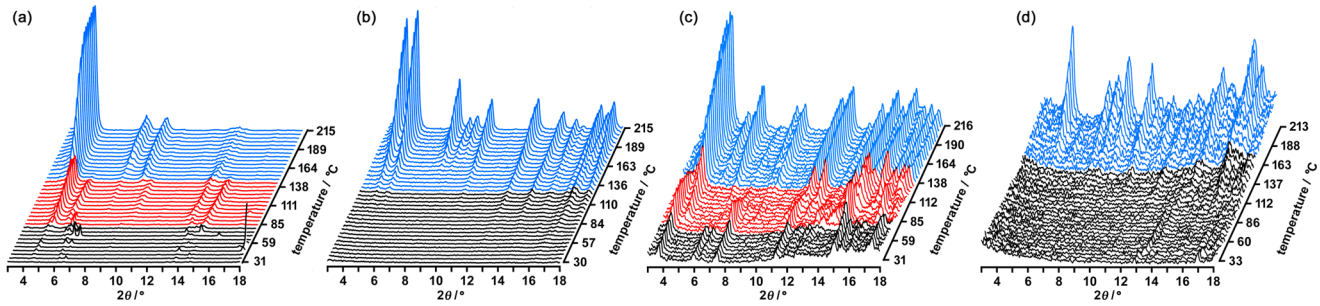

Figure 7. Changes of PXRD patterns (λ = 1.54056 Å) of (a) **Tp-2Ds**, (b) **T12-1**, (c) **T18-1**, and (d) **Ex-1** upon heating from room temperature to ca. 215 °C. Patterns colored red and blue correspond to the intermediate phase and solvent-removed apo-phase, respectively. Temperature was increased at the rate of 1 °C/min. PXRD patterns were recorded from 3° to 18° of 2θ with the scan rate of 3°/min. Therefore, each scan has a temperature gradient of 5 °C. Since the as-formed crystal of **Tp** includes either , two, or three forms of **Tp-1**, **Tp-2**, and **Tp-3**, we will refer to the crystalline bulk as **Tp-2Ds**.

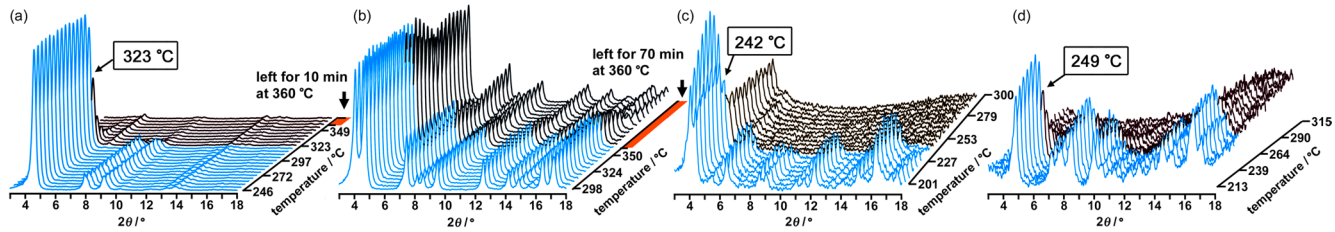

Figure 8. Changes of PXRD patterns (λ = 1.54056 Å) of the apo-crystals upon further heating: (a) **Tp-apo**, (b) **T12-apo**, (c) **T18-apo-I**, and (d) **Ex-apo**.

124TCB = 1/6 for **T12-1**; **T18**/MeBz = 1/6 for **T18-1**; and **Ex**/124TCB = 1/9.5 for **Ex-1**. In all cases, TG curves showed weight loss corresponding to complete removal of the solvent molecules included in the frameworks, and reached a flat region at around 200 °C.

Tp-2Ds and **T12-1** show second weight losses starting at around 360 and 380 °C, respectively, combined with endothermic peaks in differential thermal analysis (DTA) curves, indicating that thermal decomposition of the compounds occurs. Indeed, the resulting materials were insoluble for common organic solvents. Remarkably, the DTA curve of **T18-1** shows a sharp exothermic peak at 254 °C. Such a sharp exothermic profile is typical for 1,4-diyne contained macrocycles and is ascribable to a thermal reaction, such as random polymerization of the 1,4-butadiyne moieties or graphenization.[26] The resulting black material was again insoluble for common organic solvents. **Ex-1** shows no significant exothermic peak in the DTA curve or a second rapid weight loss in the TG curve. However, the sample turned into a black material due to thermal decomposition after increasing the temperature to 300 °C.

Structural Changes upon Desolvation. To investigate the structural changes upon removal of the aromatic molecules from the void space, as-formed crystalline bulks of **Tp-2Ds**, **T12-1**, **T18-1**, and **Ex-1** were subjected to powder X-ray diffraction (PXRD) measurements with gradual heating. Figure 7 shows changes of the PXRD patterns of the as-formed crystalline bulks upon heating under air (1 °C/min). It was surprising that the pattern of the as-formed crystals showed almost no recognizable peaks, particularly in the case of **T12-1** and **Ex-1** that were crystallized with 124TCB. This observation is a result of the significantly low electron diffraction contrast provided by the low density H-HexNet frameworks composed of no metal but low-weight elements such as C, H, O, and highly disordered solvent molecules within the void spaces. Indeed, the diffraction peaks became unambiguous upon heating as the solvent molecules were removed.[27]

The patterns of **Tp-2Ds** at relatively low temperature (30–85 °C) show a few peaks with low intensity and their changes appear unregulated. Subsequently, unambiguous peaks at 4.92°, 5.90°, 9.8°, 13.6, and 14.8° appeared and grew from 85 °C. These peaks are not in agreement with those of **Tp-1**, **Tp-2**, or **Tp-3** crystals, indicating that a new intermediate phase (**Tp-int**) was formed.

Although it is difficult to isolate pure crystalline powder of **Tp-int**, the ^{1}H NMR spectrum of **Tp-int** indicates a stoichiometry of **Tp** and MeBz in a 1:3.5 ratio (Figure S15). The peaks ascribable to **Tp-int** were consequently replaced by new peaks including a significant peak at 4.6° and moderate ones at 8.0° and 9.2°. Intensity of the new peaks reached a plateau at 184 °C. Since ^{1}H NMR spectroscopy and TG analysis revealed that the second phase included no MeBz molecules at all, the phase was named **Tp-apo**. In the case of **T12-1**, upon heating to 215 °C, clear peaks gradually appeared with good signal/noise ratio: two significant peaks at 4.06° and 4.77° of 2θ, and 10 other peaks in the range from 5° to 18°, which are ascribable to the desolvated phase **T12-apo**. Complete removal of the solvent molecules in **T12-apo** was confirmed by ^{1}H NMR spectroscopy and TG analysis. **T18-1** yielded an intermediate phase in the range from 85 to 110 °C, and subsequently attained a solvent-free phase (**T18-apo-I**). Peaks attributed to **T18-apo-I** appeared at 4.1°, 4.4°, 6.4°, 8.9°, 11.5°, and 12.2° whose intensity was relatively weak, indicating low crystallinity. Furthermore, the yellow powder sample of **T18-1** turned a dark color before complete desolvation due to partial decomposition. **Ex-1** yielded the desolvated phase **Ex-apo** upon heating to ca. 180 °C. Peaks attributed to **Ex-apo** appeared at 4.84°, 7.2°, 7.8°, 8.5°, and 10.0°. However, the intensity of the peaks is significantly weak, even though the measurement conditions were the same as the others. DMF-

DOI: 10.1021/jacs.6b02968
J. Am. Chem. Soc. 2016, 138, 6617–6628

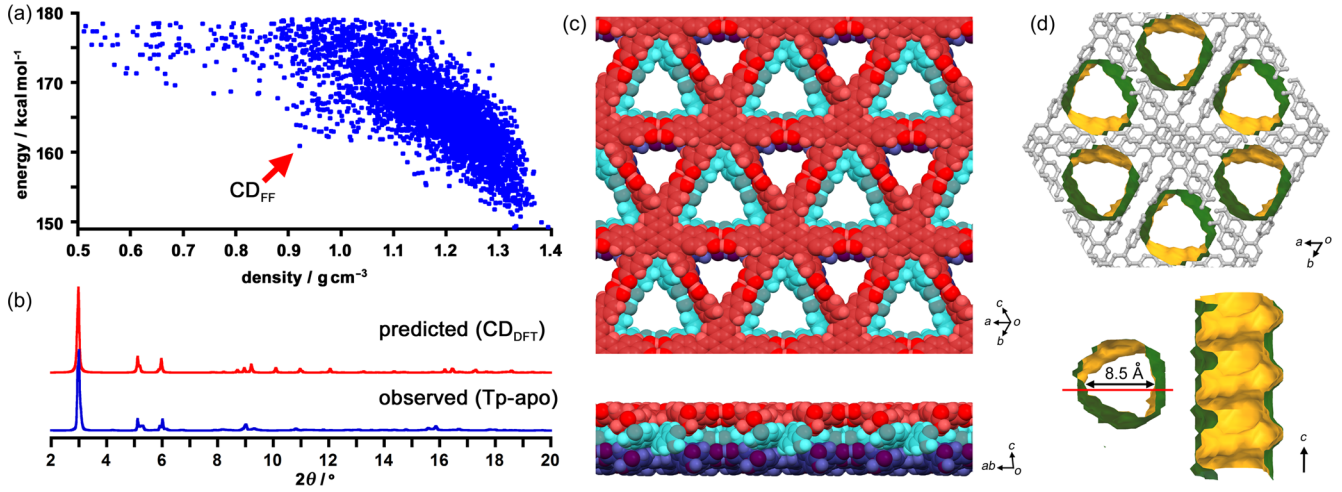

Figure 9. Candidate structures of **Tp-apo** obtained by the crystal structure prediction (CSP) technique. (a) Lattice energy vs density plot of the generated crystal structures, where CD_{FF} indicates the most appropriate candidate of **Tp-apo** judging from the similarity in the PXRD patterns. (b) PXRD patterns (λ = 0.9994 Å) of **Tp-apo** (bottom) and CD_{DTF}, which was obtained by DFT-optimization of CD_{FF} (top). (c) Top and side views of three layer packing diagrams of CD_{DFT}. (d) Visualized surface of one-dimensional pores (top) and cross-sectional view along the red line (bottom).

inserted crystals **T12-2**(DMF) and **T18-2**(DMF) also gave the same desolvated phases as in the case of **T12-1** and **T18-1**, respectively (Figure S19).

To investigate heat resistant properties of the apo-phases, **Tp-apo**, **T12-apo**, **T18-apo-I**, and **Ex-apo** were subjected to continuous PXRD measurements (Figure 8) with further heating. Peaks at 4.92° of **Tp-apo** started to decay at ca. 323 °C. The differential thermal analysis (DTA) curve of **Tp-apo** shows a weak exothermic peak at a similar temperature (346 °C), indicating a transition from **Tp-apo** to another phase. **T12-apo** shows no changes of the PXRD pattern up to 360 °C, which is the temperature limitation of the TV-PXRD apparatus. When the sample was left at 360 °C for 70 min, the peak intensity slightly decreased. It is noteworthy that remarkable heat resistance up to 360 °C was observed for the compound containing reactive acetylene moieties such as **T12**, although partial decomposition might start at this temperature, judging from the DTA curve. **T18-apo-I**, on the other hand, showed rapid changes in the PXRD pattern at ca. 242 °C due to thermal decomposition. After the thermal reaction, a broad peak at 4.7° remained, indicating that a structure with only long periodicity was formed. **Ex-1** shows complete decay of the PXRD pattern at 249 °C due to thermal decomposition of the compound.

To obtain the apo-structures under milder conditions, we also attempted desolvation by soaking in benzene at room temperature and subsequent removal of the exchanged solvent under vacuum conditions (0.2 kPa) at 40−100 °C [solvent exchange (SE-) method]. As a result, the SE-method resulted in apo-phases with the same powder diffraction patterns as those in Figure 7, except for the case of **T18** which shows a different PXRD profile (**T18-apo-II**) from that of **T18-apo-I** (Figure S20). In the following experiment on the apo-structures, we used the desolvated samples prepared by the SE-method.

Structural Investigation of the Apo-Phases. To characterize structures of the apo-phases, powder X-ray diffraction analysis was attempted. The structure of **T12-apo** was successfully revealed, while that of **T18-apo** and **Ex-apo** could not be solved because of their low crystallinity. The structure of **Tp-apo** was estimated by a crystal structure prediction (CSP) method as follows.

Candidate Structure of Tp-apo. Structural analysis of **Tp-apo** based on the experimental PXRD data failed despite our great efforts. While the intensity of the peaks in the low angle region looked fine, indexing of the diffraction data gave no authentic cell parameters, presumably due to overlap of peaks and/or existence of two or more structures. Alternatively, we applied a CSP technique to elucidate the structure. The calculation was performed by using a geometrically optimized molecular model of **Tp** with the *PPM* conformation (see Supporting Information for details). Figure 9a shows lattice energy-density mapping of approximately 5500 crystal structures belonging to the $P\bar{1}$ space group generated by Monte Carlo calculations and the subsequent force field optimization. We carefully compared the PXRD patterns of the generated structures and experimental **Tp-apo** and found that one candidate structure (CD_{FF}), indicated by a red arrow in Figure 9a, exhibits a PXRD pattern that was quite similar to the observed one. The structural parameters are a = 22.93 Å, b = 22.93 Å, c = 7.66 Å, α = 95.04°, β = 79.30°, γ = 59.62°, V = 3420.23 Å^3, lattice energy E = 160.87 kcal/mol, and density d = 0.9214 g·cm^{-3}. The structure of CD_{FF} was further optimized by DFT calculation at the vdW-DF2 level[28] with the Quantum Espresso program.[29] The parameters of the optimized structure (CD_{DFT}) were estimated to be a = 22.52 Å, b = 22.52 Å, c = 7.14 Å, α = 105.05°, β = 78.90°, γ = 59.99°, and V = 2900.87 Å^3. The CD_{DFT} nicely reproduces the diffraction peaks of **Tp-apo** in the low-angle region as shown in Figure 9b. Interestingly, CD_{DFT} exhibits a layered structure of H-HexNet sheets with permanent porosity as shown in Figure 9c. In the structure, the adjacent **Tp** cores are stacked with large overlap and triangular channels with a diameter of ca. 8.5 Å running along the c axis. The accessible volume of the pore is 33%.

Crystal Structure of T12-apo. The diffraction pattern of **T12-apo** was preliminary indexed as a monoclinic system (a = 20.135 Å, b = 43.391 Å, c = 7.4093 Å, β = 90.488°). Subsequently, the unit cell was refined by the Pawley method and assigned to space group Cn (#9). The crystal structure solution was carried out by the Monte Carlo/parallel tempering method with the geometrically optimized molecular model, giving an appropriate structure. The subsequent full pattern refinement was performed by the Rietveld method against the

DOI: 10.1021/jacs.6b02968
J. Am. Chem. Soc. 2016, 138, 6617−6628

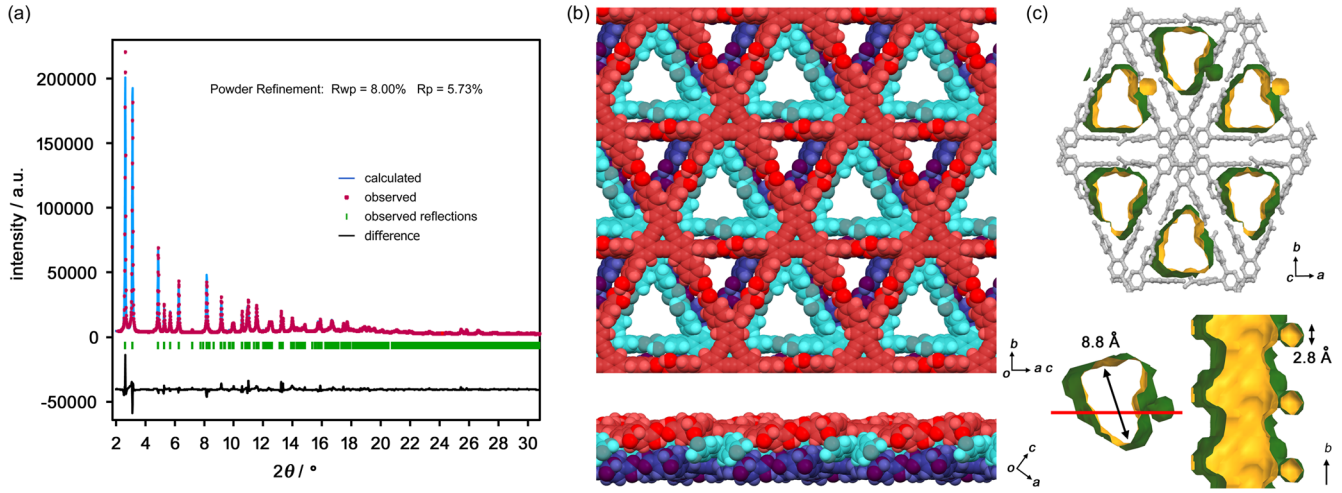

Figure 10. Structural analysis of **T12-apo**. (a) The Rietveld refinement of **T12-apo**: experimental (red) and refined (light blue) PXRD patterns, with the difference plot (black), and the reflection positions (green tick marks). (b) Top and side views of three layer packing diagrams of **T12-apo**. (c) Visualized surface of one-dimensional pores (top) and cross-sectional view along the red line (bottom).

experimental powder pattern, resulting in converging refinements with the following values [a = 20.13(2) Å, b = 43.36(4) Å, c = 7.401(7) Å, β = 90.509(4)°, R_p = 5.73%, R_{wp} = 8.00%] as shown in Figure 10a. The analysis indicates that **T12-apo** retains a layered structure of H-HexNet sheets, although hydrogen-bonded dimers of the carboxy phenyl groups are deformed.

The stacking manner of the layers is similar to that in **T12-1**: the **T12** cores are overlapped with an interplanar distance of 3.16 Å through a $\pi\cdots\pi$ interaction. It is noteworthy that two kinds of one-dimensional pores with a triangular cross section with diameter of 8.8 Å are formed along the c axis as shown in Figure 10c. One of them has a branched small spherical room with a diameter of 2.8 Å. The accessible volume of **T12-apo** is 38%. The remaining crystallinity of the LA-H-HexNet structure and the permanent porosity in **T12-apo** is indicated from the fact that **T12-1** and **T12-apo** have quite similar stacking geometries of the **T12** cores.

Optical Properties of Tp, T12, T18, and Ex in the Solid State. Optical properties of LA-H-HexNet crystals composed of C_3PIs were investigated. Figure 11 shows fluorescence spectra of the as-formed crystals and the activated apo-crystals. **Tp-apo** exhibits a structureless emission band at 416 nm (ϕ_F = 15%). **T12-apo** exhibits an emission band with vibration structure (λ = 496, 526, 546, and 590 nm, ϕ_F = 25%). **T18-apo** and **Ex-apo** show broad emission bands at 487 and 466 nm, respectively, with relatively weak intensities (ϕ_F = 5.5%, and ϕ_F = 8.0%, respectively). It is noteworthy that **T12-apo** shows the same spectral profile as **T12-1** in the emission wavelength. This indicates that the stacking manner between the **T12** cores basically remains unaltered by desolvation of **T12-1**, which is consistent with the results of crystallographic analysis on **T12-apo** and **T12-1**. Emission bands of **Tp-apo**, **T18-apo-II**, and **Ex-apo**, on the other hand, are red-shifted by 20, 22, and 14 nm, respectively, compared with their as-formed crystals **Tp-2Ds**, **T18-1**, and **Ex-1**. This implies that overlap between the C_3PI cores became larger upon desolvation-induced structural changes, although the structures of **T18-apo** and **Ex-apo** remain crystallographically unclear.

Gas Sorption. The permanent porosity of **Tp-apo**, **T12-apo**, **T18-apo-II**, and **Ex-apo** was evaluated by N_2, CO_2, and H_2 sorption−desorption measurements at 77, 195, and 77 K,

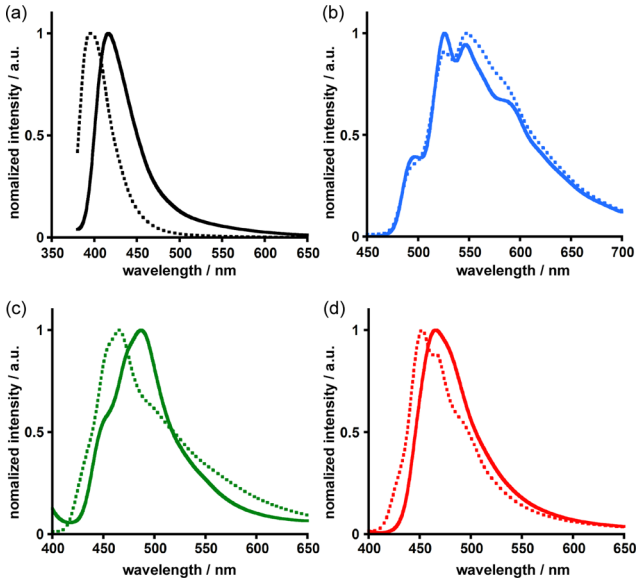

Figure 11. Normalized solid state fluorescence spectra of (a) **Tp-apo** (solid line) and **Tp-2Ds** (dashed line), (b) **T12-apo** (solid line) and **T12-1** (dashed line), (c) **T18-apo-II** (solid line) and **T18-1** (dashed line), and (d) **Ex-apo** (solid line) and **Ex-1**(dashed line).

respectively (Figure 12). **Tp-apo** has a type-I N_2 sorption isotherm at 77 K with an uptake of 187 cm^3 g^{-1} (8.35 mmol/g) at p/p_0 = 0.99 and a specific surface area SA_{BET} = 718 m^2 g^{-1} calculated by the Brunauer−Emmett−Teller model.

Other apo-crystals, on the other hand, show less significant sorption behavior [**T12-apo**: 85.4 cm^3 g^{-1} (3.81 mmol g^{-1}) at p/p_0 = 1.00. **T18-apo-II**: 44.9 cm^3 g^{-1} (2.01 mmol g^{-1}) at p/p_0 = 0.99. **Ex-1**: 41.5 cm^3 g^{-1} (1.85 mmol g^{-1}) at p/p_0 = 1.00]. Low uptake of N_2 is often observed for porous molecular crystals such as hydrogen-bonded organic frameworks (HOFs) and non-covalene organic frameworks (nCOFs).[9h] The pore size distributions of **Tp-apo** and **T12-apo** were calculated by nonlocal density functional theory (NL-DFT) methods (Figures S23 and S24). **Tp-apo** and **T12-apo** exhibit a peak at 0.77 and 0.75 nm, respectively, which is in good agreement with the candidate structure of **Tp-apo** (CD_{DFT}) obtained from the CSP calculation and the **T12-apo** structure refined by

DOI: 10.1021/jacs.6b02968
J. Am. Chem. Soc. 2016, 138, 6617−6628

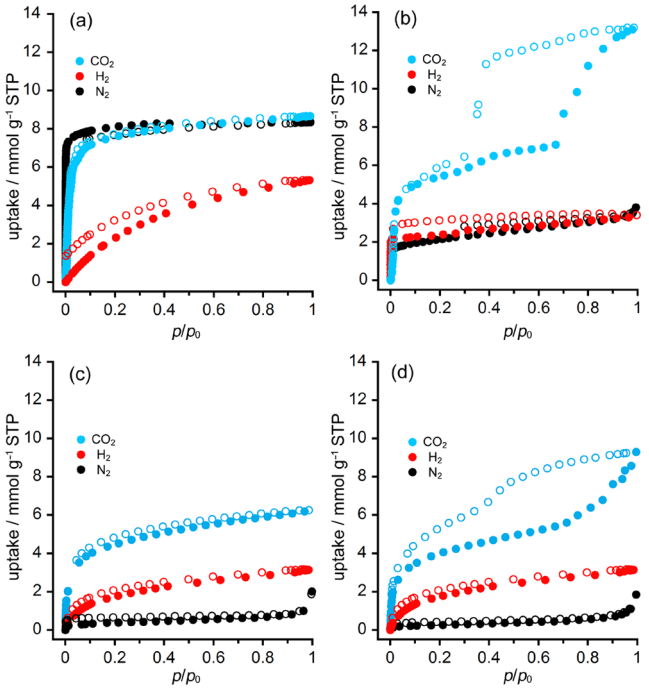

Figure 12. N_2 (77 K, black), CO_2 (195 K, light blue), and H_2 (77 K, red) sorption isotherms of (a) **Tp-apo**, (b) **T12-apo**, (c) **T18-apo-II**, and (d) **Ex-apo**. Solid symbols, sorption; open symbols, desorption.

powder X-ray analysis. For H_2 gas, **Tp-apo**, **T12-apo**, **T18-apo-II**, and **Ex-apo** show similar type-I sorption isotherms. More strictly, the isotherm of **T12-apo** reached a step at lower relative pressure ($p/p_0 < 1.0 \times 10^{-3}$), indicating the existence of micropores suitable for sorption of H_2 gas molecules. The isotherms of **Tp-apo** and **T12-apo** at 77 K revealed H_2 uptakes of 1.02 and 0.68 wt %, respectively, at 1 bar.

In contrast to N_2, CO_2 gas was adsorbed more in **T12-apo**, **T18-apo**, and **Ex-apo**, except for **Tp-apo**, due to its quadrupolar nature[30,31] in addition to smaller kinetic diameter (3.3 Å for CO_2 vs 3.6 Å for N_2). **Tp-apo** has a type-I sorption isotherm with an uptake of 194 $cm^3\ g^{-1}$ (8.67 mmol g^{-1}) at $p/p_0 = 0.99$ and a calculated SA_{BET} with 788 $m^2\ g^{-1}$, which is quite similar to the case of N_2 sorption. **T18-apo-II** also shows a type-I isotherm with an uptake of 140.6 $cm^3\ g^{-1}$ (6.28 mmol g^{-1}) at $p/p_0 = 1.01$.

T12-apo, on the other hand, shows a stepped sorption profile ($p/p_0 = 0.67$) with hysteric behavior, which is a typical-IV profile. It is generally recognized that such hysteresis is generated from (1) capillary condensation taking place in mesopores[32] or (2) framework flexibility and the existence of molecular gates, which are reported in flexible porous materials such as MOF and HOF.[33] The total uptake is 295.1 $cm^3\ g^{-1}$ (13.2 mmol g^{-1}) at $p/p_0 = 1.01$, corresponding to 13.4 CO_2 mol/**T12** mole, and 2.2 CO_2 mol per mole of the carboxyphenyl moieties. The calculated SA_{BET} based on the CO_2 sorption isotherm is 557 $m^2\ g^{-1}$. A CO_2 isotherm of **Ex-apo** includes both profiles of type-I and -II, as well as a hysteric profile with an uptake of 208.0 $cm^3\ g^{-1}$ (9.29 mmol g^{-1}) at $p/p_0 = 1.00$. This sorption profile indicates that **Ex-apo** has both micropores and nonporous or macroporous moieties, which is consistent with its low crystallinity providing weak and broad peaks in the PXRD pattern.

Vapor Sorption of Hydrocarbons. Since **Tp-apo** and **T12-apo** are revealed to retain porosity and crystallinity, these two were subjected to vapor sorption experiments at 298 K with a series of low molecular weight hydrocarbons (Figure 13). **Tp-apo** and **T12-apo** basically show similar sorption

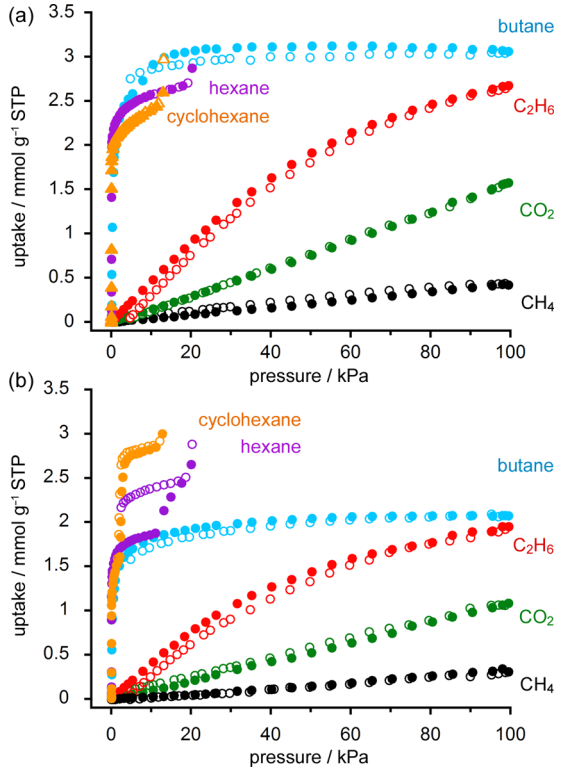

Figure 13. Hydrocarbon sorption isotherms of (a) **Tp-apo** and (b) **T12-apo** at 298.15 K (methane, black circle; CO_2, green circle; ethane, red circle; *n*-butane, light blue circle; *n*-hexane, purple circle; cyclohexane, yellow triangle. Solid symbols, sorption; open symbols, desorption).

behaviors. Isotherms for methane (kinetic diameter: 3.8 Å) and ethane (3.9 Å), as well as CO_2 show sorption profiles with gentle uptake over wide range of the pressure. In the case of *n*-butane (4.3 Å), on the other hand, **Tp-apo** and **T12-apo** show typical type-I isotherms with a sharp rise and the attainment of the saturation capacity of 3.1 and 2.1 mmol g^{-1}, respectively. These results indicate that hydrocarbon as large as or larger than butane enables a favorable van der Waals interaction to adsorb in the channel.[34] It is noteworthy that **Tp-apo** showed the maximum amount of uptake (3.1 mmol g^{-1}) in the case of butane, while **T12-apo** showed that (3.0 mmol g^{-1}) in the case of cyclohexane (6.0 Å). These results indicate that a size and/or shape of **T12-apo**'s pore is more suitable to accommodate bulky hydrocarbons compared with **Tp-apo**.

Finally, to reveal water resistance, crystalline powders of **Tp-apo** and **T12-apo** were subjected to moisture under a saturated vapor pressure condition at 50 °C for 22 h and for 10 h, respectively. Their PXRD patterns after exposed moisture showed no changes in intensity and profile (Figures S25 and S26). Furthermore, we revealed that crystalline powders of **Tp-apo** and **T12-apo** experienced no structural collapse, even when the powders were soaked into boiling water at least for 5 h (Figures S27 and S28). These results indicate that the present LA-H-HexNets (**Tp-apo** and **T12-apo**) have resistance against water probable owing to hydrophobic $\pi\cdots\pi$ interactions between C_3PI cores and a multiple hydrogen bonds.

DOI: 10.1021/jacs.6b02968
J. Am. Chem. Soc. 2016, 138, 6617−6628

CONCLUSION

In conclusion, this is the first demonstration that a series of C_3-symmetric π-conjugated planar molecules (**Tp**, **T12**, **T18**, and **Ex**) with three 4,4′-dicarboxy-*o*-terphenyl moieties in their periphery are networked through the phenylene triangle (PhT) motif to form robust hydrogen-bonded hexagonal networks (H-HexNets) with dual or triple pores. The H-HexNets stack without interpenetration to yield layered assemblies of the H-HexNets (LA-H-HexNets) with accessible volumes in the range of 45−59%. Furthermore, the desolvated LA-H-HexNets of **Tp** and **T12** exhibit high crystallinity, heat resistance up to ca. 320 and 360 °C, respectively, and permanent porosity after desolvation: SA_{BET} = 788 and 557 m^2 g^{-1}, respectively, based on CO_2 sorption at 195 K. We believe that the present design principle can be applied to construct a wide range of two-dimensional noncovalent organic frameworks (2D-nCOFs) and create a pathway to developing a new class of porous organic materials.

ASSOCIATED CONTENT

Supporting Information

The Supporting Information is available free of charge on the ACS Publications website at DOI: 10.1021/jacs.6b02968.

Experimental details, synthetic procedures, spectroscopy, detailed crystal structures of **Tp-1**, **T12-1**, **T18-1**, **Ex-1**, **T12-2**(DMF) and **T18-2**(DMF), and non-HexNet crystals, determination of host/guest ratio, thermal analysis, moisture resistance, conformational interpretation of a C_3PI (PDF)

Crystallographic data for **T12-1** (CIF)

Crystallographic data for **Ex-1** (CIF)

Crystallographic data for **T12-2**(DMF) (CIF)

Crystallographic data for **T12-1D** (CIF)

Crystallographic data for **T12-apo_CD-DFT** (CIF)

Estimated structure of **Tp-apo_CD$_{DFT}$** (CIF)

AUTHOR INFORMATION

Corresponding Author

*hisaki@mls.eng.osaka-u.ac.jp

Notes

The authors declare no competing financial interest.

ACKNOWLEDGMENTS

This work was supported by Grant-in-Aid for Scientific Research (C) (T15K04591) and for Scientific Research on Innovative Areas (2601): π-System Figuration (15H00998 for I.H., 15H00990 for T.O., and 15H01006 for M.K.) from MEXT Japan. We thank Prof. H. Tsue at Kyoto University for his fruitful advice about powder X-ray diffraction analysis. Crystallographic data were collected using synchrotron radiation at the BL38B1 and BL02B2 in the SPring-8 with approval of JASRI (proposal nos. 2014B1168, 2015A1174, 2015A1193, 2015B1685, 2015B1397, and 2015B1130).

REFERENCES

(1) Slater, A. G.; Cooper, A. I. *Science* **2015**, *348*, 988.

(2) (a) Li, M.; Li, D.; O'Keeffe, M.; Yaghi, O. M. *Chem. Rev.* **2014**, *114*, 1343−1370. (b) Carlucci, L.; Ciani, G.; Proserpio, D. M.; Mitina, T. G.; Blatov, V. A. *Chem. Rev.* **2014**, *114*, 7557−7580.

(3) (a) Feng, X.; Ding, X.; Jiang, D. *Chem. Soc. Rev.* **2012**, *41*, 6010−6022. (b) Ding, S.-Y.; Wang, W. *Chem. Soc. Rev.* **2013**, *42*, 548−568. (c) Waller, P. J.; Gándara, F.; Yaghi, O. M. *Acc. Chem. Res.* **2015**, *48*, 3053−3063.

(4) (a) Stock, N.; Biswas, S. *Chem. Rev.* **2012**, *112*, 933−969. (b) Cook, T. R.; Zheng, Y.-R.; Stang, P. J. *Chem. Rev.* **2013**, *113*, 734−777.

(5) (a) Tozawa, T.; Jones, J. T. A.; Swamy, S. I.; Jiang, S.; Adams, D. J.; Shakespeare, S.; Clowes, R.; Bradshaw, D.; Hasell, T.; Chong, S. Y.; Tang, C.; Thompson, S.; Parker, J.; Trewin, A.; Bacsa, J.; Slawin, A. M. Z.; Steiner, A.; Cooper, A. I. *Nat. Mater.* **2009**, *8*, 973−978. (b) Mastalerz, M. *Chem. - Eur. J.* **2012**, *18*, 10082−10091. (c) Tian, J.; Thallapally, P. K.; McGrail, B. P. *CrystEngComm* **2012**, *14*, 1909−1919.

(6) (a) Côté, A. P.; Benin, A. I.; Ockwig, N. W.; O'Keeffe, M.; Matzger, A. J.; Yaghi, O. M. *Science* **2005**, *310*, 1166−1170. (b) Guo, J.; Xu, Y.; Jin, S.; Chen, L.; Kaji, T.; Honsho, Y.; Addicoat, M. A.; Kim, J.; Saeki, A.; Ihee, H.; Seki, S.; Irle, S.; Hiramono, M.; Gao, J.; Jiang, D. *Nat. Commun.* **2013**, *4*, 2736. (c) Dogru, M.; Handloser, M.; Auras, F.; Kunz, T.; Medina, D.; Hartschuh, A.; Knochel, P.; Bein, T. *Angew. Chem., Int. Ed.* **2013**, *52*, 2920−2924. (d) Chen, T.-H.; Popov, I.; Kaveevivitchai, W.; Chuang, Y.-C.; Chen, Y.-S.; Daugulis, O.; Jacobson, A. J.; Miljanić, O. Š. *Nat. Commun.* **2014**, *5*, 5131.

(7) (a) Ermer, O.; Neudörfl, J. *Chem. - Eur. J.* **2001**, *7*, 4961−4980. (b) Ermer, O.; Neudörfl, J. *Helv. Chim. Acta* **2001**, *84*, 1268−1313. (c) Ma, B.-Q.; Coppens, P. *Chem. Commun.* **2003**, 2290−2291.

(8) (a) Dogru, M.; Handloser, M.; Auras, F.; Kunz, T.; Medina; Hartschuh, A.; Knochel, P.; Bein, T. *Angew. Chem., Int. Ed.* **2013**, *52*, 2920−2924. (b) Calik, M.; Auras, F.; Salonen, L. M.; Bader, K.; Grill, I.; Handloser, M.; Medina, D. D.; Dogru, M.; Löbermann, F.; Trauner, D.; Hartschuh, A.; Bein, T. *J. Am. Chem. Soc.* **2014**, *136*, 17802−17807.

(9) (a) Melendez, R. E.; Sharma, C. V. K.; Zaworotko, M. J.; Bauer, C.; Rogers, R. D. *Angew. Chem., Int. Ed. Engl.* **1996**, *35*, 2213−2215. (b) Palmans, A. R. A.; Vekemans, J. A. J. M.; Kooijman, H.; Spek, A. L.; Meijer, E. W. *Chem. Commun.* **1997**, 2247−2248. (c) Maspoch, D.; Domingo, N.; Ruiz-Molina, D.; Wurst, K.; Tejada, J.; Rovira, C.; Veciana, J. *J. Am. Chem. Soc.* **2004**, *126*, 730−731. (d) Sozzani, P.; Bracco, S.; Comotti, A.; Ferretti, L.; Simonutti, R. *Angew. Chem., Int. Ed.* **2005**, *44*, 1816−1820. (e) Saha, B. K.; Jetti, R. K. R.; Reddy, L. S.; Aitipamula, S.; Nangia, A. *Cryst. Growth Des.* **2005**, *5*, 887−899. (f) Bhogala, B. R.; Nangia, A. *Cryst. Growth Des.* **2006**, *6*, 32−35. (g) Men, Y.-B.; Sun, J.; Huang, Z.-T.; Zheng, Q.-Y. *Angew. Chem., Int. Ed.* **2009**, *48*, 2873−2876. (h) Luo, X.-Z.; Jia, X.-J.; Deng, J.-H.; Zhong, J.-L.; Liu, H.-J.; Wang, K.-J.; Zhong, D.-C. *J. Am. Chem. Soc.* **2013**, *135*, 11684−11687.

(10) Duchamp, D. J.; Marsh, R. *Acta Crystallogr., Sect. B: Struct. Crystallogr. Cryst. Chem.* **1969**, *25*, 5−19.

(11) Herbstein, F. H.; Kapon, M.; Reisner, G. M. *J. Inclusion Phenom.* **1987**, *5*, 211−214.

(12) Weber, E.; Hecker, M.; Koepp, E.; Orlia, W.; Czugler, M.; Csöregh, I. *J. Chem. Soc., Perkin Trans. 2* **1988**, 1251−1257.

(13) Despite interpenetration, some of HexNets still retain porosity, see: (a) Bajpai, A.; Venugopalan, P.; Moorthy, J. N. *CrystEngComm* **2014**, *16*, 4853−4860. (b) Zentner, C. A.; Lai, H. W. H.; Greenfield, J. T.; Wiscons, R. A.; Zeller, M.; Campana, C. F.; Talu, O.; FitzGerald, S. A.; Rowsell, J. L. C. *Chem. Commun.* **2015**, *51*, 11642−11645. (c) Lai, H. W. H.; Wiscons, R. A.; Zentner, C. A.; Zeller, M.; Rowsell, J. L. C. *Cryst. Growth Des.* **2016**, *16*, 821−833.

(14) Kobayashi, K.; Shirasaka, T.; Horn, E.; Furukawa, N. *Tetrahedron Lett.* **2000**, *41*, 89−93.

(15) (a) Kobayashi, K.; Shirasaka, T.; Sato, A.; Horn, E.; Furukawa, N. *Angew. Chem., Int. Ed.* **1999**, *38*, 3483−3486. (b) Kobayashi, K.; Sato, A.; Sakamoto, S.; Yamaguchi, K. *J. Am. Chem. Soc.* **2003**, *125*, 3035−3045. (c) Maly, K. E.; Gagnon, E.; Maris, T.; Wuest, J. D. *J. Am. Chem. Soc.* **2007**, *129*, 4306−4322.

(16) Kobayashi, K.; Kobayashi, N.; Ikuta, M.; Therrien, B.; Sakamoto, S.; Yamaguchi, K. *J. Org. Chem.* **2005**, *70*, 749−752.

(17) (a) Zhou, T.-Y.; Xu, S.-Q.; Wen, Q.; Pang, Z.-F.; Zhao, X. *J. Am. Chem. Soc.* **2014**, *136*, 15885−15888. (b) Zhu, Y.; Wan, S.; Jin, Y.; Zhang, W. *J. Am. Chem. Soc.* **2015**, *137*, 13772−13775. (c) Baldwin, L. A.; Crowe, J. W.; Shannon, M. D.; Jaroniec, C. P.; McGrier, P. L.

DOI: 10.1021/jacs.6b02968
J. Am. Chem. Soc. 2016, 138, 6617−6628

Chem. Mater. **2015**, *27*, 6169−6172. (d) Xu, A.-Q.; Zhan, T.-G.; Wen, Q.; Pang, Z.-F.; Zhao, X. *ACS Macro Lett.* **2016**, *5*, 99−102. (e) Yang, H.; Du, Y.; Wan, S.; Trahan, G. D.; Jin, Y.; Zhang, W. *Chem. Sic.* **2015**, *6*, 4049−4053.

(18) (a) Bonifazi, D.; Mohnani, S.; Llanes-Pallas, A. *Chem. - Eur. J.* **2009**, *15*, 7004−7025. (b) Kudernac, T.; Lei, S.; Elemans, J. A. A. W.; De Feyter, S. *Chem. Soc. Rev.* **2009**, *38*, 402−421.

(19) Hisaki, I.; Nakagawa, S.; Tohnai, N.; Miyata, M. *Angew. Chem., Int. Ed.* **2015**, *54*, 3008−3012.

(20) Hisaki, I.; Ikenaka, N.; Tohnai, N.; Miyata, M. *Chem. Commun.* **2016**, *52*, 300−303.

(21) Juricek, M.; Kouwer, P. H. J.; Rehak, J.; Sly, J.; Rowan, A. E. *J. Org. Chem.* **2009**, *74*, 21−25.

(22) Crystal data for **T12−1**: $2(C_{66}H_{36}O_{12})\cdot(C_5H_3Cl_3)$, F_w = 2223.46, a = 15.3981(2) Å, b = 21.2475(2) Å, c = 23.5028(2) Å, α = 67.6497(6)°, β = 76.3614(6)°, γ = 83.8777(7)°, V = 6910.01(13) Å^3, T = 93 K, triclinic, space group $P\bar{1}$, Z = 2, 44 868 collected, 22 405 unique (R_{int} = 0.033) reflections, the final R1 and wR2 values 0.107 ($I > 2.0\sigma(I)$) and 0.336 (all data), respectively. Crystal data of **Ex-1**: $(C_{90}H_{48}O_{12})\cdot 8.5(C_6H_3Cl_3)$, F_w = 2863.68, a = 15.3971(11) Å, b = 17.5779(9) Å, c = 26.0548(13) Å, α = 88.620(4)°, β = 87.381(5)°, γ = 65.012(6)°, V = 6384.9(7) Å^3, T = 100 K, triclinic, space group $P\bar{1}$, Z = 2, 178 734 collected, 49 133 unique (R_{int} = 0.144) reflections, the final R1 and wR2 values 0.141 ($I > 2.0\sigma(I)$) and 0.432 (all data), respectively. CCDC numbers: **T12-1** (CCDC-1457115) and **Ex-1** (CCDC- -1457116) contain the supplementary crystallographic data for this paper. These data can be obtained free of charge from The Cambridge Crystallographic Data Centre via www.ccdc.cam.ac.uk/.

(23) Atomic radii were adopted as follows: 1.20 (H), 1.70 (C), 1.52 (O). The probe radius was 1.2 Å.

(24) Although stacking manner of most of 2D-COFs have been reported to be an eclipse AA arrangement, other arrangements such as serrated and inclined are proposed, see: Lukose, B.; Kuc, A.; Heine, T. *Chem. - Eur. J.* **2011**, *17*, 2388−2392.

(25) Unfortunately, it is not clear whether as-formed bulk crystals of LA-H-HexNets of **Tp** have **Tp-1**, **Tp-2**, or **Tp-3** structure, because a general diffractometer in laboratory provided only weak and ambiguous XRD patterns due to the low electron density contrast generated by disordered MeBz molecules within the pores. Therefore, such bulk crystals obtained by crystallization at 100 °C are called as **Tp-2Ds**.

(26) (a) Hisaki, I.; Sakamoto, Y.; Shigemitsu, H.; Tohnai, N.; Miyata, M. *Cryst. Growth Des.* **2009**, *9*, 414−420. (b) Hisaki, I.; Kometani, E.; Shigemitsu, H.; Saeki, A.; Seki, S.; Tohnai, N.; Miyata, M. *Cryst. Growth Des.* **2011**, *11*, 5488−5497. (c) Hisaki, I.; Manabe, N.; Osaka, K.; Saeki, A.; Seki, S.; Tohnai, N.; Miyata, M. *Bull. Chem. Soc. Jpn.* **2014**, *87*, 323−333.

(27) Comotti, A.; Bracco, S.; Sozzani, P.; Horike, S.; Matsuda, R.; Chen, J.; Takata, M.; Kubota, Y.; Kitagawa, S. *J. Am. Chem. Soc.* **2008**, *130*, 13664−13672.

(28) Lee, K.; Murray, E. D.; Kong, L.; Lundqvist, B. I.; Langreth, D. C. *Phys. Rev. B: Condens. Matter Mater. Phys.* **2010**, *82*, 081101−4.

(29) (a) Giannozzi, P.; Baroni, S.; Bonini, N.; Calandra, M.; Car, R.; Cavazzoni, C.; Ceresoli, D.; Chiarotti, G. L.; Cococcioni, M.; Dabo, I.; Dal Corso, A.; de Gironcoli, S.; Fabris, S.; Fratesi, G.; Gebauer, R.; Gerstmann, U.; Gougoussis, C.; Kokalj, A.; Lazzeri, M.; Martin-Samos, L.; Marzari, N.; Mauri, F.; Mazzarello, R.; Paolini, S.; Pasquarello, A.; Paulatto, L.; Sbraccia, C.; Scandolo, S.; Sclauzero, G.; Seitsonen, A. P.; Smogunov, A.; Umari, P.; Wentzcovitch, R. M. *J. Phys.: Condens. Matter* **2009**, *21*, 39550. (b) Quantum Espresso Home Page, http://www.quantum-espresso.org.

(30) Hisaki, I.; Yasumiya, D.; Shigemitsu, H.; Tsuzuki, S.; Tohnai, N.; Miyata, M. *Phys. Chem. Chem. Phys.* **2012**, *14*, 13918−13921.

(31) (a) Yang, W.; Greenaway, A.; Lin, X.; Matsuda, R.; Blake, A. J.; Wilson, C.; Lewis, W.; Hubberstey, P.; Kitagawa, S.; Champness, N. R.; Schröder, M. *J. Am. Chem. Soc.* **2010**, *132*, 14457−14469. (b) Lü, J.; Perez-Krap, C.; Suyetin, M.; Alsmail, N. H.; Yan, Y.; Yang, S.; Lewis, W.; Bichoutskaia, E.; Tang, C. C.; Blake, A. J.; Cao, R.; Schröder, M. *J. Am. Chem. Soc.* **2014**, *136*, 12828−12831.

(32) (a) Sing, K. S. W.; Everett, D. H.; Haul, R. A. W.; Moscou, L.; Pierotti, R. A.; Rouquérol, J.; Siemieniewska, T. *Pure Appl. Chem.* **1985**, *57*, 603−619.

(33) (a) Henke, S.; Schneemann, A.; Wutscher, A.; Fischer, R. A. *J. Am. Chem. Soc.* **2012**, *134*, 9464−9474. (b) He, Y.; Xiang, S.; Chen, B. *J. Am. Chem. Soc.* **2011**, *133*, 14570−14573.

(34) (a) Ogoshi, T.; Sueto, R.; Yoshikoshi, K.; Yamagishi, T. *Chem. Commun.* **2014**, *50*, 15209−15211. (b) Ogoshi, T.; Sueto, R.; Yoshikoshi, K.; Sakata, Y.; Akine, S.; Yamagishi, T. *Angew. Chem., Int. Ed.* **2015**, *54*, 9849−9852.

DOI: 10.1021/jacs.6b02968
J. Am. Chem. Soc. 2016, 138, 6617−6628